On the Westward Turning of Hurricane Sandy (2012): Effect of Atmospheric Intraseasonal Oscillations

LIUDAN DING

Key Laboratory of Meteorological Disaster, Ministry of Education/Joint International Research Laboratory of Climate and Environmental Change/Collaborative Innovation Center on Forecast and Evaluation of Meteorological Disasters, Nanjing University of Information Science and Technology, Nanjing, China

TIM LI

International Pacific Research Center, and Department of Atmospheric Sciences, School of Ocean, Earth Science and Technology, University of Hawai'i at Mānoa, Honolulu, Hawaii, and Key Laboratory of Meteorological Disaster, Ministry of Education/Joint International Research Laboratory of Climate and Environmental Change/Collaborative Innovation Center on Forecast and Evaluation of Meteorological Disasters, Nanjing University of Information Science and Technology, Nanjing, China

BAOQIANG XIANG

NOAA/Geophysical Fluid Dynamics Laboratory, Princeton, New Jersey, and University Corporation for Atmospheric Research, Boulder, Colorado

MELINDA PENG[a]

General Dynamics Information Technology/Naval Research Laboratory, Monterey, California

(Manuscript received 2 October 2018, in final form 10 July 2019)

ABSTRACT

Hurricane Sandy (2012) experienced an unusual westward turning and made landfall in New Jersey after its northward movement over the Atlantic Ocean. The landfall caused severe casualties and great economic losses. The westward turning took place in the midlatitude Atlantic where the climatological mean wind is eastward. The cause of this unusual westward track is investigated through both observational analysis and model simulations. The observational analysis indicates that the hurricane steering flow was primarily controlled by atmospheric intraseasonal oscillation (ISO), which was characterized by a pair of anticyclonic and cyclonic circulation systems. The anticyclone to the north was part of a global wave train forced by convection over the tropical Indian Ocean through Rossby wave energy dispersion, and the cyclone to the south originated from the tropical Atlantic through northward propagation. Hindcast experiments using a global coupled model show that the model is able to predict the observed circulation pattern as well as the westward steering flow 6 days prior to Sandy's landfall. Sensitivity experiments with different initial dates confirm the important role of the ISO in establishing the westward steering flow in the midlatitude Atlantic. Thus the successful numerical model experiments suggest a potential for extended-range dynamical tropical cyclone track predictions.

1. Introduction

Hurricanes are disastrous weather systems and may pose substantial economic and societal threats for the U.S. coastline (Pielke et al. 2008). Many studies have been conducted to understand the mechanisms of hurricane genesis, track, and intensification. Several factors may affect hurricane tracks, including environmental steering flow (Chan and Gray 1982), planetary vorticity gradient, and storm size and structure (Holland 1983; Li and Zhu 1991). Forecast challenges during tropical cyclone (TC) recurvature and sudden turns arise from complex interactions with topography, the

[a] Current affiliation: University of Colorado Colorado Springs, Colorado Springs, Colorado.

Corresponding author: Tim Li, timli@hawaii.edu

DOI: 10.1175/JCLI-D-18-0663.1

North Atlantic Ocean subtropical high (Chen et al. 2001), a monsoon gyre (Carr and Elsberry 1990; Bi et al. 2015), and/or atmospheric low-frequency motions (Liu et al. 2018).

The intraseasonal oscillation (ISO) is one of the primary low-frequency modes in the atmosphere. The main characteristic of the ISO in northern winter in the tropics is the eastward propagation of a large-scale convective envelope along the equator. This boreal winter ISO mode is often referred to as the Madden–Julian oscillation (MJO), because it was first discovered by Madden and Julian (1971, 1972), who found a statistically significant peak in equatorial zonal wind on intraseasonal time scales. Although its main convective system is located in the tropics, the MJO may exert a significant effect on weather and climate phenomena in the midlatitudes such as the North Atlantic Oscillation through Rossby wave energy propagation (Matthews et al. 2004; Cassou 2008; Lin et al. 2009; Seo and Son 2012; Henderson et al. 2017). In contrast to boreal winter, the ISO activity in boreal summer is mostly confined in the Indo-Pacific monsoon region, with pronounced northward propagation (e.g., Jiang et al. 2004; Li 2014). It has been shown that the boreal summer ISO may significantly impact TC genesis in the western North Pacific Ocean through its modulation of the monsoon trough [see Li (2012) for a review]. Physically, the ISO may affect TC genesis through barotropic energy conversion (Sobel and Maloney 2000; Hartmann and Maloney 2001; Maloney and Dickinson 2003; Hsu et al. 2011), modulation of background moisture and vorticity (Cao et al. 2014), and impacts on precursory synoptic disturbances such as synoptic-scale wave trains (Lau and Lau 1990; Li 2006; Zhou and Li 2010), easterly waves (Tam and Li 2006; Frank and Roundy 2006), and TC energy dispersion–induced Rossby wave trains (Li et al. 2003; Li and Fu 2006). The control of the ISO on TC genesis has been extensively studied in different tropical basins (e.g., Maloney 2000; Maloney and Hartmann 2000; Mo 2000; Fu et al. 2007; Li and Zhou 2013; Lee et al. 2018; Zhao and Li 2019).

In addition to its modulation of TC genesis, the ISO may impact the TC track. Using a nondivergent barotropic model, Carr and Elsberry (1995) demonstrated that a TC-like vortex experiences a sudden northward turning after it interacts with a low-frequency monsoon gyre. Using the full-physics WRF Model, Bi et al. (2015) showed that the anomalous northward turning of Typhoon Megi (2010) resulted from a Fujiwhara binary interaction between the TC and a low-frequency (10–60-day) monsoon gyre. A more recent study by Liu et al. (2018) found that three types of low-frequency circulation patterns (i.e., monsoon gyre, wave trains, and midlatitude trough patterns) may interact with western North Pacific TCs. North Atlantic hurricane activities may be impacted by MJO through changes in large-scale upper-tropospheric thermal conditions and vertical wind shear (Barrett and Leslie 2009; Kossin et al. 2010; Klotzbach 2010).

Hurricane Sandy had a devastating impact on the east coast of the United States in October 2012. This high-impact TC formed over the central Caribbean Sea on 21 October and then moved northward over the Atlantic. On 29 October, it turned suddenly westward, made landfall in New Jersey, and caused property damage estimated more than $50 billion (Blake et al. 2013). Some previous studies suggested that Sandy's track was affected by changes to the midlatitude jet stream forced by Arctic amplification. However, the midlatitude effects of Arctic amplification are still under debate in the meteorological community (e.g., Barnes et al. 2013; Greene et al. 2013; Lackmann 2015; Mattingly et al. 2015). The unexpected westward turning was not predicted early on by many real-time operational forecast models and motivates us to investigate the following scientific questions: 1) What led to the westward curvature of Hurricane Sandy while the midlatitudes were controlled by prevailing westerlies? 2) What dynamic process was responsible for the unusual TC track?

In this study, we aim to address the questions above by emphasizing the roles of tropical and midlatitude ISOs in causing the unusual westward turning of Hurricane Sandy. With filtering techniques, we can separate low-frequency modes with the purpose of exploring how the ISO influences the TC track. The remaining part of this paper is organized as follows. Analysis data and general methods are described in section 2. Section 3 displays the detailed results of the observational analysis. In section 4, we discuss the results from dynamic model hindcast experiments. Conclusions are given in section 5.

2. Data and methods

a. Data

The primary observational data used for the current study are from the National Centers for Environmental Prediction (NCEP) Reanalysis I dataset (Kalnay et al. 1996). This dataset includes daily mean wind, geopotential height, and other atmospheric fields. In addition, we use daily observed outgoing longwave radiation (OLR) from the National Oceanic and Atmospheric Administration polar-orbiting satellites (Liebmann and Smith 1996). The horizontal resolution of the reanalysis and OLR datasets is 2.5° × 2.5°. The "HURDAT" dataset from the National Hurricane Center is used to show the positions of Hurricane Sandy at every 6 h prior

to Sandy's landfall on 29 October and every 4 h on 29 October (Jarvinen et al. 1984; Kieper et al. 2016).

The model data used for this study are output from hindcast experiments of the Geophysical Fluid Dynamics Laboratory (GFDL) Forecast-Oriented Low Ocean Resolution (FLOR) coupled model (Vecchi et al. 2014). A new double plume convection scheme (Zhao et al. 2018) was used in the experiments. The atmospheric model has a 50-km horizontal resolution with 32 vertical levels, and the oceanic model has a horizontal resolution of 1°. Following Chen and Lin (2013), the initial conditions were generated through a nudging technique from the NCEP Global Forecast System (GFS) analysis product (with horizontal resolution of 28 km and 6-hourly time interval) for both the atmosphere and the ocean models. This model has been demonstrated to have MJO prediction skill up to 27 days using the Real-time Multivariate MJO (RMM) index (Wheeler and Hendon 2004) as a metric (Xiang et al. 2015b). There are 25 ensemble members for the hindcast experiments. The model was integrated for one month for each member. The TC track was determined based on a commonly used method with use of combined sea level pressure, temperature, and 850-hPa vorticity fields. For more details, readers are referred to Xiang et al. (2015a).

b. Analysis methods

The Lanczos temporal filtering method was applied to extract the ISO signal. Many previous studies showed that the ISO in general has a wide spectrum range, with a typical period of 10–90 days (e.g., Sperber et al. 1997; Ding and Wang 2007). Thus, the original reanalysis and OLR fields were separated into different time scale components via Fourier decomposition (Duchon 1979), and we retained 10–90-day signals to represent the tropical and midlatitude ISOs.

In addition, the Wheeler–Kiladis space–time spectral analysis method (Wheeler and Kiladis 1999) was applied to isolate the eastward-propagating MJO signal and associated atmospheric circulation pattern. For this special mode, we kept zonal wavenumbers 1–4 and a period of 20–80 days based on the wavenumber–frequency power spectra diagram.

The outputs from the FLOR model 1-month integration with two different initial conditions on 21 and 23 October were analyzed. To compare the model-simulated ISO signals with the observed counterpart, a nonfiltering method was applied because of the limited integration length, following Hsu et al. (2015) and Bi et al. (2015). The following is the specific procedure. 1) The reanalysis data 22 days prior to the initial forecast time were attached to the 30-day forecast data. 2) A 5-day running mean was then applied to the modified dataset above to remove the synoptic and shorter time scales (with a period of less than 10 days). 3) A 45-day running mean (equivalent to a 90-day-or-longer period) was then subtracted from the newly generated dataset at step 2 above to remove the annual cycle and other scales longer than 90-day period. With this approach, an approximate 10–90-day low-frequency signal was obtained from the model integration, and the result was then compared with the observation.

c. Idealized modeling experiment

An anomaly atmospheric general circulation model (AGCM) was employed to understand atmospheric response to a specified heating. The anomaly AGCM was developed based on the GFDL global spectrum dry AGCM (Held and Suarez 1994). It has been used for various studies including asymmetric atmospheric response to an equatorially symmetric El Niño forcing in the Asian monsoon region (Wang et al. 2003), atmospheric precursory signals associated with MJO initiation (Jiang and Li 2005), the formation mechanism of synoptic-scale wave trains in the western North Pacific (Li 2006), and the seasonal contrast of El Niño teleconnection patterns between winter and summer (Zhu and Li 2016).

The model uses sigma ($\sigma = p/p_s$) as its vertical coordinate and there are five evenly distributed sigma levels with an interval of 0.2, a top level at $\sigma = 0$, and a bottom level at $\sigma = 1$. The horizontal resolution is T42. Observed October climatological mean fields derived from the NCEP–NCAR reanalysis were prescribed as the model basic state. An anomaly heating resembling the observed OLR pattern associated with the MJO over the tropical Indian Ocean and western Pacific was specified. The heating has an idealized vertical profile with the maximum heating rate in the midtroposphere. The anomaly AGCM was integrated for 60 days. The averaged fields during the last 20 days are used to represent the equilibrium response to the heating.

3. Role of the ISO in the westward steering flow

The column-integrated climatological mean wind from 850 to 200 hPa shows pronounced eastward steering flow in the midlatitude Atlantic in October (Fig. 1a). To understand the unusual movement of Sandy in this late season within a generally westerly environment, we first examined actual 850–200-hPa integrated steering flow on the turning day of Sandy (i.e., 29 October) as shown in Fig. 1b. Indeed, a westward steering flow appeared over the midlatitude Atlantic near the coast of New Jersey on this date. This implies that the westward

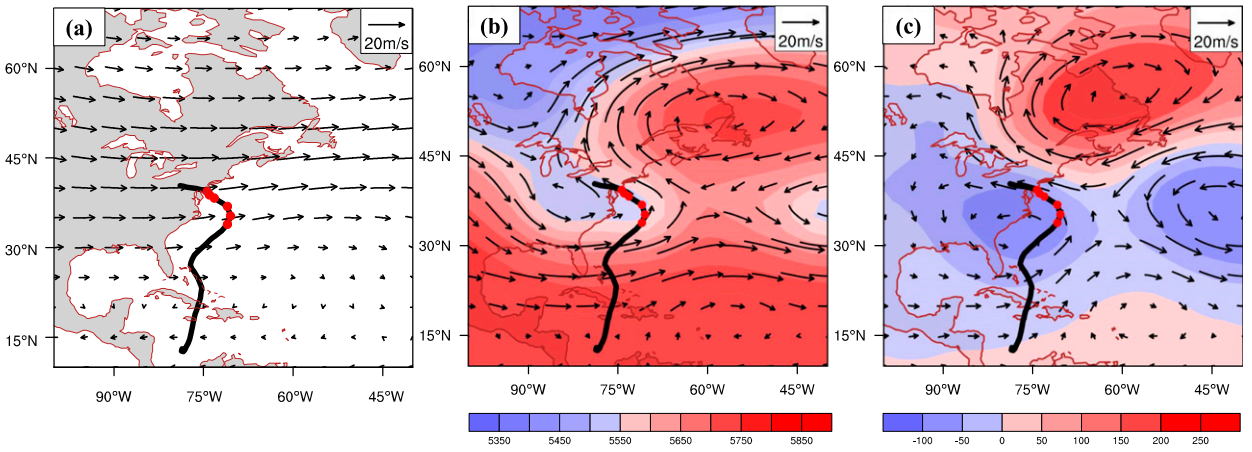

FIG. 1. Horizontal patterns of column-integrated (850–200 hPa) (a) climatological mean wind, (b) actual wind, and (c) 10–90-day filtered wind fields (vectors; m s^{-1}) on 29 Oct 2012. The corresponding 500-hPa geopotential height fields (gpm) are shaded in (b) and (c). Black curves indicate Sandy's trajectories from genesis to landfall, and red dots represent Sandy's 4-hourly locations on 29 Oct.

TC steering flow arose from the atmospheric transient motion.

One important component of the transient motion is the atmospheric intraseasonal oscillation (ISO). Figure 1c shows the 850–200-hPa integrated steering-flow component attributed to the ISO, calculated based on the 10–90-day Lanczos filtered wind field. Note that there is great similarity between the original unfiltered (Fig. 1b) and the 10–90-day filtered (Fig. 1c) wind field. Both fields show a marked meridional dipole, with anticyclonic flow to the north and cyclonic flow to the south. The resemblance between the two fields suggests that the ISO played an important role in setting up the westward steering flow on 29 October.

In addition, steering flow associated with synoptic-scale motion (e.g., upper-tropospheric trough) may also play a role. To quantitatively measure the relative contributions of the ISO and synoptic-scale motion, we defined a latitude–longitude box covering the area from 32.5° to 42.5°N and from 67.5° to 77.5°W. Then we calculated the TC steering flow in this key transition region on 29 October associated with the total wind field, the ISO component, and the non-ISO component (which consists of the climatological annual cycle and synoptic-scale and other transient motions excluding the ISO). The zonal steering flow from the total field is −3.1 m s^{-1}, while the zonal steering flow due to the ISO (non-ISO component) is −10.1 m s^{-1} (+7.0 m s^{-1}). Among the non-ISO components the annual cycle steering flow is +11.1 m s^{-1} while synoptic-scale steering flow is −4.2 m s^{-1}. The calculated total steering flow from the observation is very close to Sandy's observed forward speed. A similar result was obtained when a vertical integration of 850–300- or 500-hPa wind field was used to represent the steering flow (see Table 1). The result indicates that the ISO played a primary role in causing Sandy's westward track.

Next, we examined the evolution of the ISO circulation pattern prior to Sandy's westward turning. Figure 2 shows 10–90-day filtered low-level wind and OLR fields on 23, 25, 27, and 29 October. It is interesting to note that a negative OLR anomaly and a cyclonic circulation center appeared in the tropical Atlantic (near 20°N, 75°W) on 23 October. In subsequent days, the enhanced convective center and the cyclone moved northward and strengthened. On 29 October, the cyclonic circulation system was located in midlatitudes near 35°N, 75°W. Hurricane Sandy was affected by the easterly wind to the north of the cyclone. Therefore the northward propagation of the tropical convection and circulation

TABLE 1. Zonal steering flow (m s^{-1}) represented by 850–200-hPa integration, 850–300-hPa integration, and 500-hPa wind field averaged over 32.5°–42.5°N, 67.5°–77.5°W on 29 Oct 2012, derived from the low-frequency background state (LFBS; greater than 90 days), 10–90-day filtered ISO, and high-frequency (HF; less than 10 days) component, respectively.

	LFBS (>90 days)	Filtered (10–90 days)	HF (<10 days)	Actual
850–200 hPa	11.1	−10.1	−4.2	−3.1
850–300 hPa	9.5	−9.6	−2.8	−2.9
500 hPa	11.6	−11.9	−2.1	−2.4

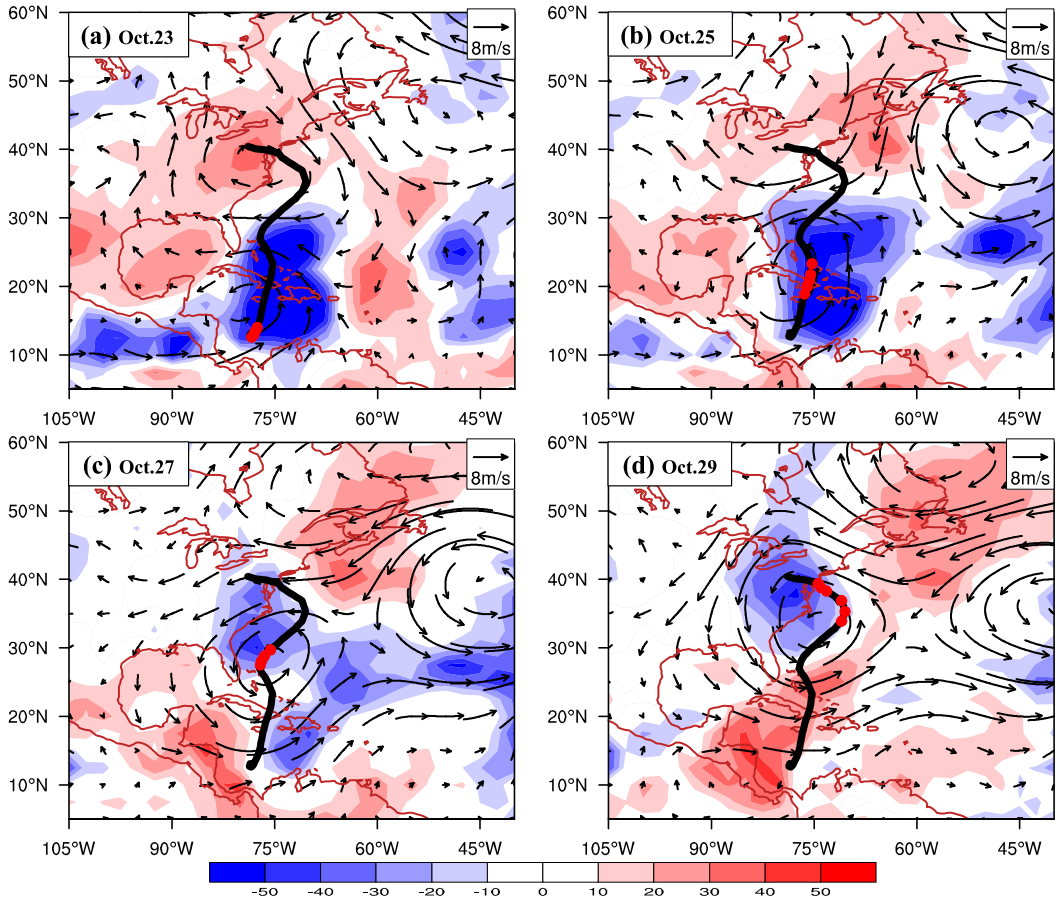

FIG. 2. Horizontal patterns of 10–90-day filtered OLR (shading; W m^{-2}) and 850-hPa wind (vectors; m s^{-1}) fields on (a) 23, (b) 25, (c) 27 and (d) 29 Oct 2012. The black lines indicate Sandy's trajectories from genesis to landfall, and the red dots represent Sandy's 6-hourly (or 4-hourly) locations.

associated with the ISO was critical in generating the intraseasonal cyclonic circulation system as part of the meridional dipole structure.

To illustrate the coherent northward propagation, we plotted the time–latitude section of 10–90-day filtered OLR and 850-hPa vorticity fields averaged from 70° to 80°W. Figure 3 shows a clear match between the OLR and vorticity fields. Both the enhanced convection and cyclonic vorticity propagated from low latitudes to middle latitudes from 21 October to 29 October.

While the southern branch of the dipole circulation pattern appeared to originate from the tropical Atlantic, our analysis suggested that the northern branch was a result of remote forcing from the tropical Indian Ocean. It is noted from Figs. 1 and 2 that a pronounced anticyclone appeared north of 40°N. The easterly winds between the northern anticyclone and the southern cyclone prompted the unusual westward track of Hurricane Sandy on 29 October. Figure 4 shows filtered OLR and 200-hPa geopotential height fields on 21, 23, 25, 27, and 29 October respectively. These fields were obtained through a space–time power spectrum analysis to retain eastward-propagating planetary-scale MJO signals, following Wheeler and Kiladis (1999). This global upper-tropospheric circulation pattern indicates that the anticyclone was a part of a global wave train that originated from the tropical Indian Ocean.

Figure 4 demonstrates that there was a prominent MJO signal in the tropics a few days prior to Sandy's landfall. The MJO signal in the tropics was characterized by a negative OLR center over the tropical Indian Ocean basin and it propagated eastward from 21 to 29 October. The diabatic heating associated with the MJO stimulated Rossby wave energy source and the wave energy propagated poleward and eastward, forming a big circle (Hoskins and Karoly 1981). The Rossby wave energy dispersion can be inferred from the alternating positive and negative geopotential height centers in the upper troposphere (200 hPa). As seen in Fig. 4, the wave train excited by the MJO in the tropical

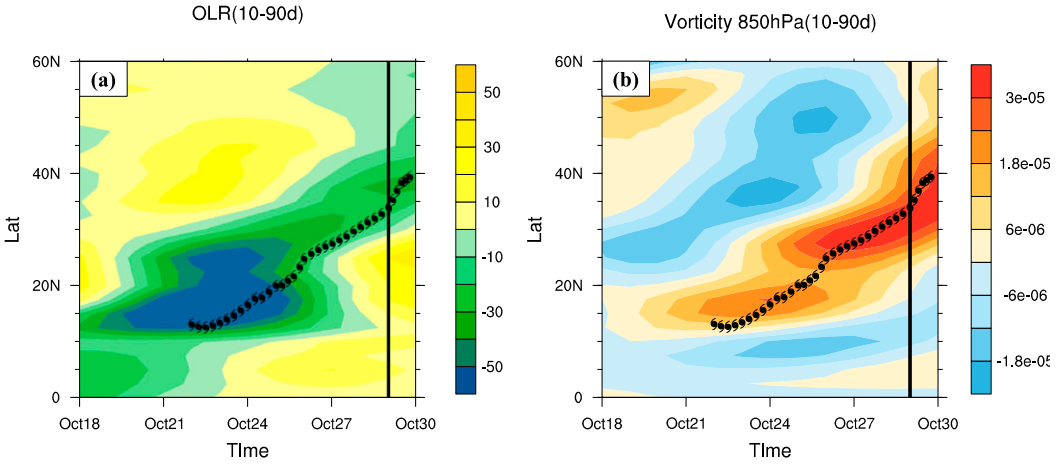

FIG. 3. Latitude–time sections of 10–90-day filtered (a) OLR (shading; $\mathrm{W\,m^{-2}}$) and (b) 850-hPa vorticity (shading; $\mathrm{s^{-1}}$) averaged over 70°–80°W. The vertical black lines indicate the day of westward turning. The hurricane symbols represent Sandy's 6-hourly (or 4 hourly on 29 Oct) locations.

Indian Ocean spread northeastward crossing the Asian continent and Pacific, inducing a positive geopotential height anomaly over the east coast of North America. The positive geopotential height anomaly moved slowly eastward, as the MJO heat source in the tropical Indian Ocean moved slowly toward the east.

The wave train exhibited an equivalent barotropic vertical structure in the mid- to high latitudes. Figure 5 shows the zonal–vertical cross section of the geopotential height anomaly averaged along 45°–60°N. The maximum amplitude of the geopotential height anomaly appears in the upper troposphere (near 200 hPa), and it decreases toward the surface.

To identify the source of the wave train and its energy dispersion characteristics, we calculated the perturbation Rossby wave source (RWS) (Sardeshmukh and Hoskins 1988; Qin and Robinson 1993; Rodrigues and Woollings 2017) and wave activity flux (Takaya and Nakamura 2001) averaged during 23–29 October. The perturbation RWS is defined as $S' \approx -v'_\chi \cdot \nabla\overline{\zeta} - \overline{\zeta}\nabla \cdot v'_\chi$, where v'_χ is the divergent component of the anomalous horizontal velocity field at 200 hPa and $\overline{\zeta}$ means the climatological mean absolute vorticity. Although the mean absolute vorticity is small in the tropics, divergent flow is greater at the edge of the heating region and the gradient of mean absolute vorticity is larger toward higher latitudes. Our calculation reveals that strong RWS occurs along the jet-stream region (Fig. 6). In response to a positive MJO heating anomaly over the northern Indian Ocean and a negative heating anomaly over the Philippines, a pair of negative and positive RWS centers appears over subtropical Asia near 20°N, 45°E and 20°N, 100°E, respectively. The global Rossby wave train is well connected to the anomalous RWS over the region.

The formula of the Takaya–Nakamura wave activity flux may be written as

$$W = \frac{1}{2|\overline{U}|}\begin{bmatrix} \overline{u}(\psi'^2_x - \psi'\psi'_{xx}) + \overline{v}(\psi'_x\psi'_y - \psi'\psi'_{xy}) \\ \overline{u}(\psi'_x\psi'_y - \psi'\psi'_{xy}) + \overline{v}(\psi'^2_y - \psi'\psi'_{yy}) \end{bmatrix},$$

where $\overline{U}$, $\overline{u}$, and $\overline{v}$ represent the climatological monthly mean horizontal, zonal, and meridional winds, ψ' denotes perturbation streamfunction, and subscripts denote partial derivatives at zonal or meridional directions. The wave activity flux represents Rossby wave energy propagation direction. Figure 6 shows that pronounced northeastward wave activity fluxes appear to the northeast of the RWS centers over the subtropical Asia. The wave activity fluxes extend northeastward along the big circle path onto the North America and North Atlantic sector. To demonstrate the role of the tropical heating in generating the large-scale wave train, we relied on the anomaly AGCM experiment. A heating distribution with a pair of positive and negative anomalies resembling the observed OLR pattern on 23 October (shown in Fig. 4) was specified. Under the October background mean flow, the model is able to reproduce a wave train pattern with alternating positive and negative geopotential height centers in upper troposphere resembling the observed (Fig. 7a). Sensitivity experiments were further carried out to reveal the relative roles of the positive and negative heating anomalies. The results showed that the positive heating is crucial (Figs. 7b,c). Thus the numerical model experiments confirm that the heating over tropical Indian Ocean associated with the MJO was the primary source that excited the global wave train oriented from subtropical Asia all the way to North Atlantic.

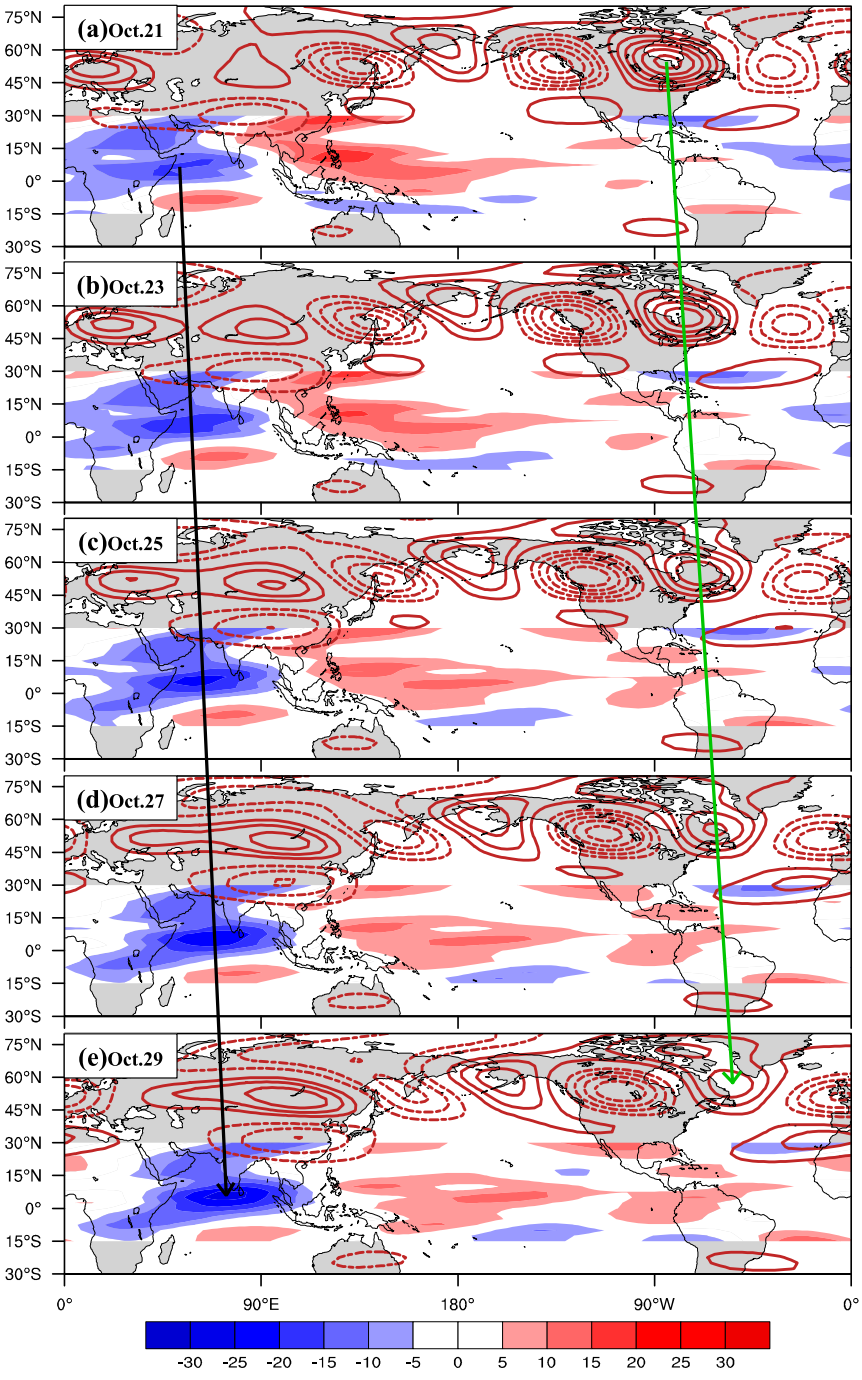

FIG. 4. Evolutions of the OLR anomaly (shading; $W\,m^{-2}$) in the tropics and 200-hPa geopotential height (contours; gpm) associated with the MJO mode on (a) 21, (b) 23, (c) 25, (d) 27, and (e) 29 Oct 2012. The black and green arrows respectively indicate the slow (at phase speed of $\sim 4\,m\,s^{-1}$) eastward movement of MJO convection over the tropical Indian Ocean and the upper-level anticyclone over the North American sector.

To sum up, the observational data analysis and numerical model simulations reveal that the low-frequency wind associated with the tropical and midlatitude ISO played an important role in causing the anomalous westward turning of Hurricane Sandy. The local circulation system was represented by an anomalous cyclone and anticyclone pair near 40°N. The cyclonic circulation to the south originated from the tropical Atlantic, whereas the anticyclonic

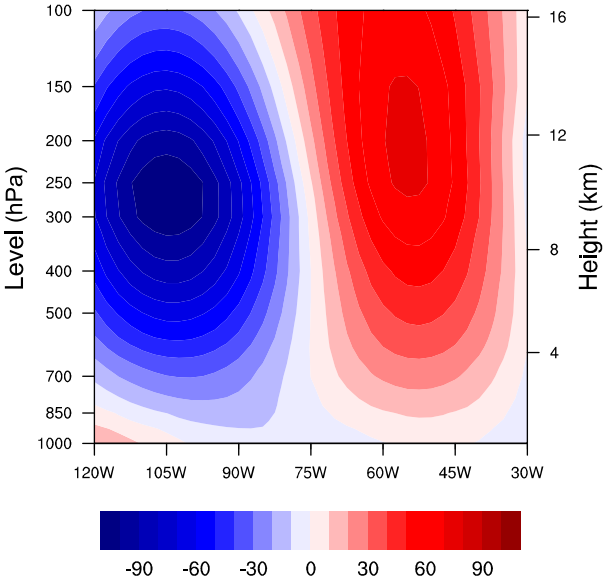

FIG. 5. Zonal–vertical cross section along 45°–60°N of MJO-related geopotential height anomaly field (shading; gpm) on 29 Oct 2012.

circulation to the north was part of a global wave train pattern triggered by the MJO heating in the tropical Indian Ocean. The strong easterly flow between the cyclone and the anticyclone steered Hurricane Sandy westward.

4. Forecast experiments

According to the analysis above, Hurricane Sandy's westward track was primarily affected by low-frequency steering flow associated with the ISO. Can the state-of-the-art climate model simulate the ISO evolution and Sandy's westward track a few days ahead? To address this question, we rely on ensemble runs of the GFDL FLOR coupled model (Xiang et al. 2015a).

Figure 8 compares Sandy's observed track from HURDAT and the track prediction with an initial condition on 21 October and 23 October. It is clearly shown that the forecast with an initial condition on 23 October (6 days prior to landfall) well predicted Sandy's westward turning, but the forecast on 21 October failed. Meanwhile, we also compared the forecast TC intensities with the observed and the result is shown in Fig. 9. As one can see, the forecast TC with the 23 October initial condition has a stronger intensity and is closer to the observed than that with the 21 October initial condition. In the following, we try to understand processes leading to the contrasting track predictions by focusing on the potential impact of ISO in the two experiments.

We first examined local circulation patterns from the observation and two predictions. Figure 10 shows 10–90-day low-frequency fields to illustrate the evolution of anomalous OLR and 850-hPa wind fields from 23 to 29 October. A marked difference appears in the northward propagation of anomalous OLR and wind fields between the two forecasts. The forecast starting on 23 October successfully captured the intensity and northward migration of the enhanced convection and the low-level cyclone, whereas the forecast with the 21 October initial condition failed to do so.

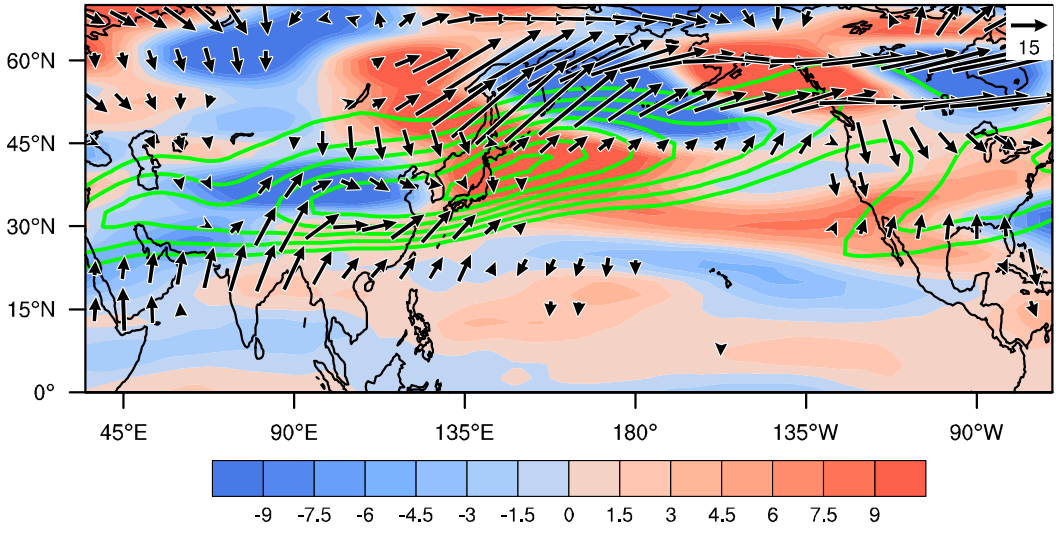

FIG. 6. Horizontal patterns of anomalous Rossby wave source (shading; 10^{-11} s^{-2}) and wave activity flux (vectors; m^2 s^{-2}; only values exceeding 3 m^2 s^{-2} are shown) averaged during 23–29 Oct 2012 and climatological October mean wind speed field at 200 hPa (green contours; m s^{-1}; 5 m s^{-1} interval, with only values exceeding 20 m s^{-1} shown). The RWS and wave activity flux were calculated from the mean and intraseasonal wind fields at 200 hPa.

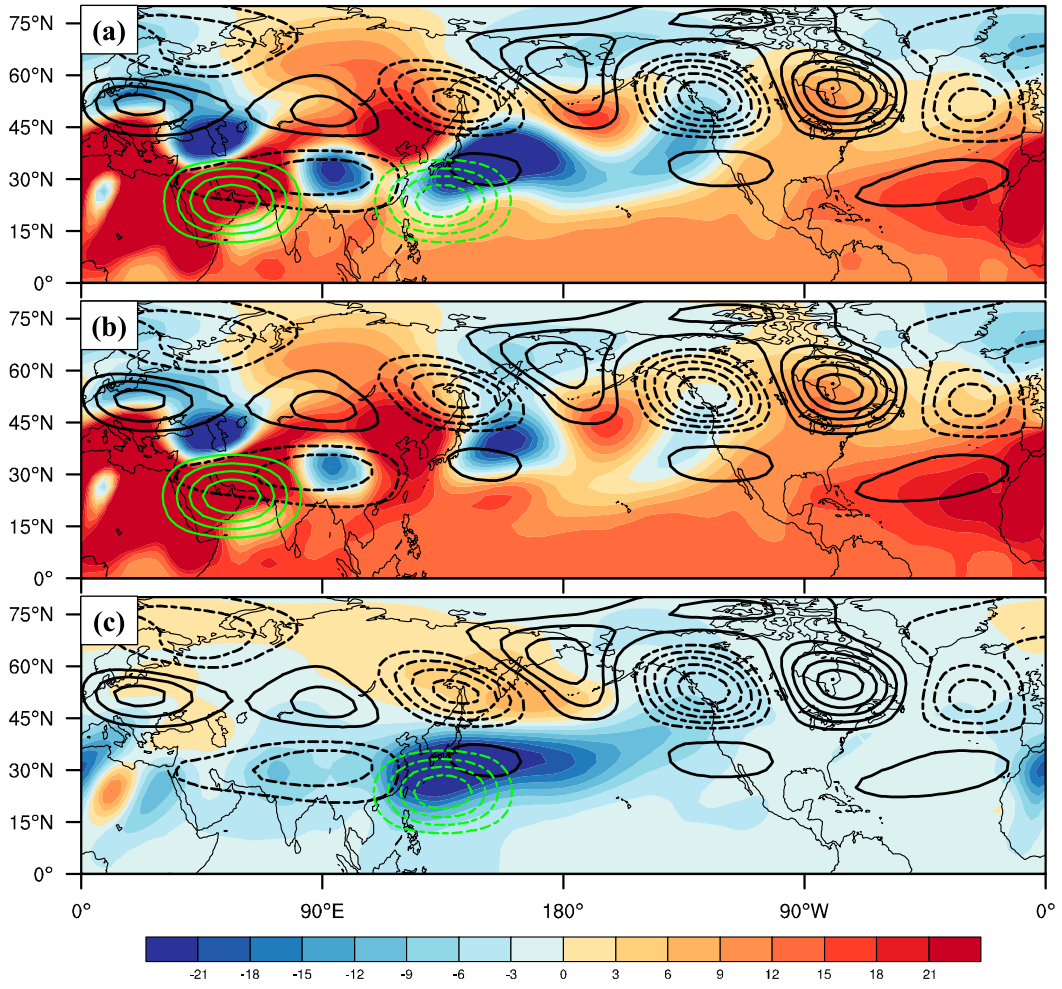

FIG. 7. The simulated 200-hPa anomalous geopotential height fields (shading; gpm) in response to (a) a pair of positive and negative heating anomalies (green contours), (b) the positive heating only, and (c) the negative heating only. For comparison, the observed 200-hPa anomalous geopotential height field on 23 Oct 2012 (black contours; gpm) is also plotted.

By comparing two forecasts in Fig. 10, one can identify that the key to the successful prediction of Sandy's track lies in whether the model is able to correctly predict the meridional dipole structure in the midlatitude Atlantic on 29 October (the rightmost panel of Fig. 10). For the forecast with the 23 October initial condition, the OLR and wind patterns resemble those from the observation. Both the location and intensity of the low-level southern cyclone and northern anticyclone were well predicted. In contrast, the forecast with the 21 October initial condition failed to capture the dipole structure. In particular, the low-frequency cyclonic flow is hardly seen.

By comparing the two forecast experiments (middle vs bottom panel), one can find the following characteristics. On the 25th, the gross patterns of the forecast wind field are very similar, even though the intensity of the wind field in the bottom panel is weaker. On the 27th, the convection and circulation anomalies are much weaker in the bottom panel compared to those in the middle panel. The difference on the 29th becomes very distinct as the convection and circulation anomalies in the bottom panel almost disappear. In sum, the forecast with the 23 October initial conditions (middle panel) was capable of predicting the characteristics of low-frequency atmospheric circulation evolution associated with the ISO very well, leading to a realistic track forecast for Hurricane Sandy at 6 days of lead time. It is worth mentioning that the forecast TC with the 21 October initial conditions appears weaker and shorter lived, implying the possible role of the northward propagating ISO cyclone flow in modulating the TC intensity.

The remote forcing from the tropical Indian Ocean, which was responsible for the establishment of an anomalous anticyclone in the North Atlantic north of 40°N, also exhibited some differences between the two experiments. Figure 11 shows 200-hPa geopotential

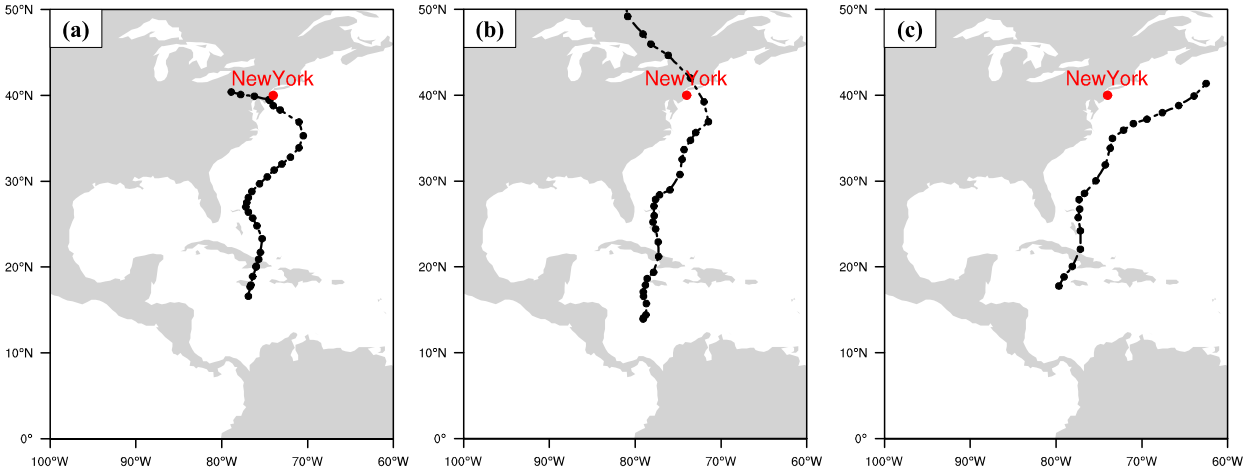

FIG. 8. Tracks of Sandy based on (a) observations from HURDAT, (b) a forecast with initial condition on 23 Oct 2012, and (c) a forecast with initial condition on 21 Oct 2012 from the GFDL global ensemble prediction system FLOR.

height and OLR anomaly fields that are MJO related on 29 October. The intensity of the OLR anomaly in the tropical Indian Ocean is weaker in the 21 October initial conditions experiment than in the 23 October initial conditions experiment. As a result, the upper-level positive geopotential height anomaly center shifts more to the north in the former, compared to the latter and in the observation. This northward shift, along with the missing of a cyclone to the south, leads to substantial underestimation of the westward low-frequency steering flow associated with the ISO and thus the failure of predicting Sandy's westward turn at the later stage.

The errors in predicting both the southern and northern parts of the local low-frequency circulation field in the North Atlantic led to a marked bias in the hurricane steering flow. Figure 12 shows the observed and forecast vertical (850–200 hPa) integrated low-frequency steering flow on 29 October. For the forecast experiment with the 23 October initial condition, the model remarkably predicted the easterly steering flow near 40°N. In contrast, the forecast with the 21 October initial condition had poor performance in predicting the local low-frequency wind field, which leads to an enormous bias in the steering flow. An eastward or much weaker westward low-frequency steering flow appears in the region. The result is consistent with the eastward track in the 21 October initial condition case. The different track forecasts support our hypothesis that the low-frequency steering flow is a main factor determining Hurricane Sandy's westward track. It also supports the claim that the ISO is important for successful hurricane track forecasting (Liu et al. 2018).

An interesting question is what caused the different performance in the two forecast experiments. We noted that the errors arose from the inaccurate representation of ISO intensity, particularly the low-level cyclonic flow anomaly, on 23 October for the 21 October initial conditions case as well as the subsequent forecast of ISO evolution from 23 October to 29 October. A further in-depth diagnosis is needed to fully address the question.

In summary, two hindcast experiments were carried out with different initial time. As compared with the

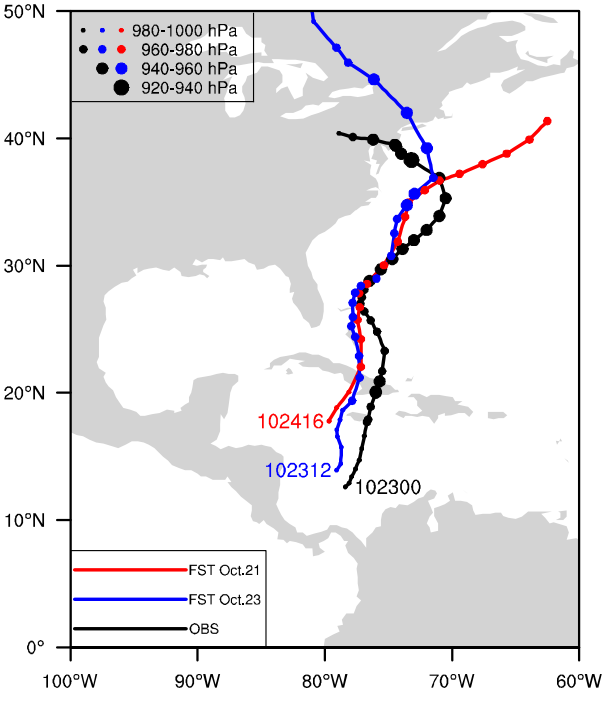

FIG. 9. Tracks and intensities of Sandy based on observations from HURDAT and forecasts from FLOR. Different sizes of the filled circles represent the intensity of Sandy. The time when Sandy's central minimum pressure dropped below 1000 hPa is also labeled.

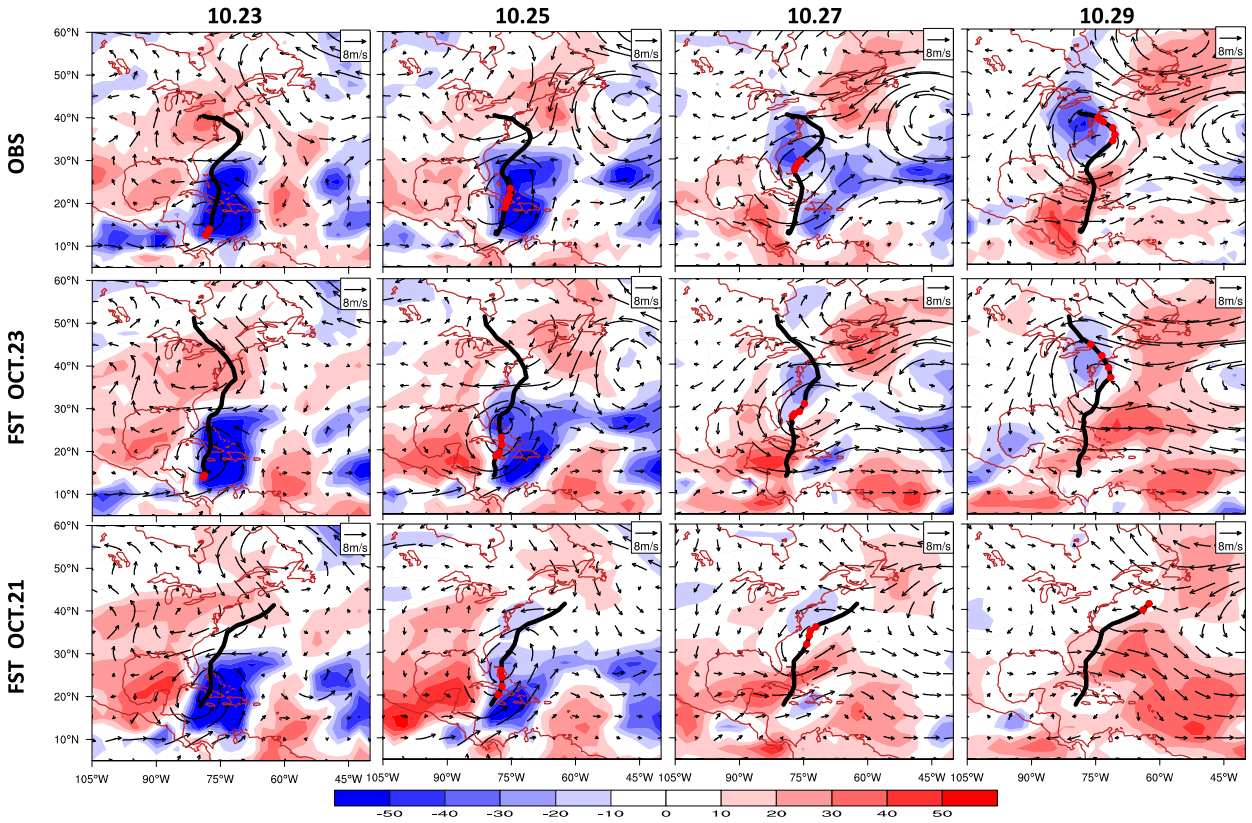

FIG. 10. Horizontal patterns of intraseasonal filtered OLR (shading; W m^{-2}) and anomalous 850-hPa wind (vectors; m s^{-1}) fields on (left) 23, (left center) 25, (right center) 27, and (right) 29 Oct 2012 for results from (top) observations and forecast results with initial conditions on (middle) 23 and (bottom) 21 Oct 2012. The black lines indicate Sandy's trajectories, and the red dots represent Sandy's locations.

21 October initial conditions, the forecast with 23 October initial conditions successfully predicts the northward propagation of the convection and wind anomalies over the Atlantic (which eventually leads to the setup of a cyclone south of 40°N) and the remote teleconnection from the tropical Indian Ocean. As a result, the model is capable of predicting the establishment of the easterly steering flow and Sandy's westward track. The hindcast experiments support the role of the ISO in extended-range forecast. Thus an accurate forecast of the ISO evolutions in the tropics and midlatitudes is crucial for Sandy's track prediction.

5. Conclusions

Hurricane Sandy (2012) was one of the highest-impact TCs over the Atlantic basin. After its formation on 22 October, it moved northward and then unusually turned to the west and made landfall in New Jersey, causing catastrophic losses and casualties. This study focuses on understanding the cause of its unusual westward track while the climatological season mean wind is westerly. It is found that a low-frequency intraseasonal westward steering flow is largely responsible for this westward track.

The diagnosis of daily reanalysis indicates that the main system affecting Sandy's track at the critical time is the low-frequency (10–90-day) ISO mode. The steering flow due to synoptic scale (less than 10 days) motion is much weaker. During the westward turning time, the local circulation over the midlatitude Atlantic is dominated by a low-frequency cyclone and anticyclone pair. The cyclone (south of 40°N) originated from the tropical Atlantic and moved northward in subsequent days, while the anticyclone (north of 40°N) was part of a global wave train triggered by the MJO originating over the tropical Indian Ocean. As a result, an easterly steering flow was generated between the low-frequency cyclone and the anticyclone, which steered Sandy to turn westward and make landfall in New Jersey.

Extended-range forecasts with an atmosphere–ocean coupled global ensemble model were carried out to understand how the Sandy forecast depends on initial conditions. The model is able to successfully forecast the westward curvature with the initial condition on 23 October but fails to do so for the forecast with 21 October

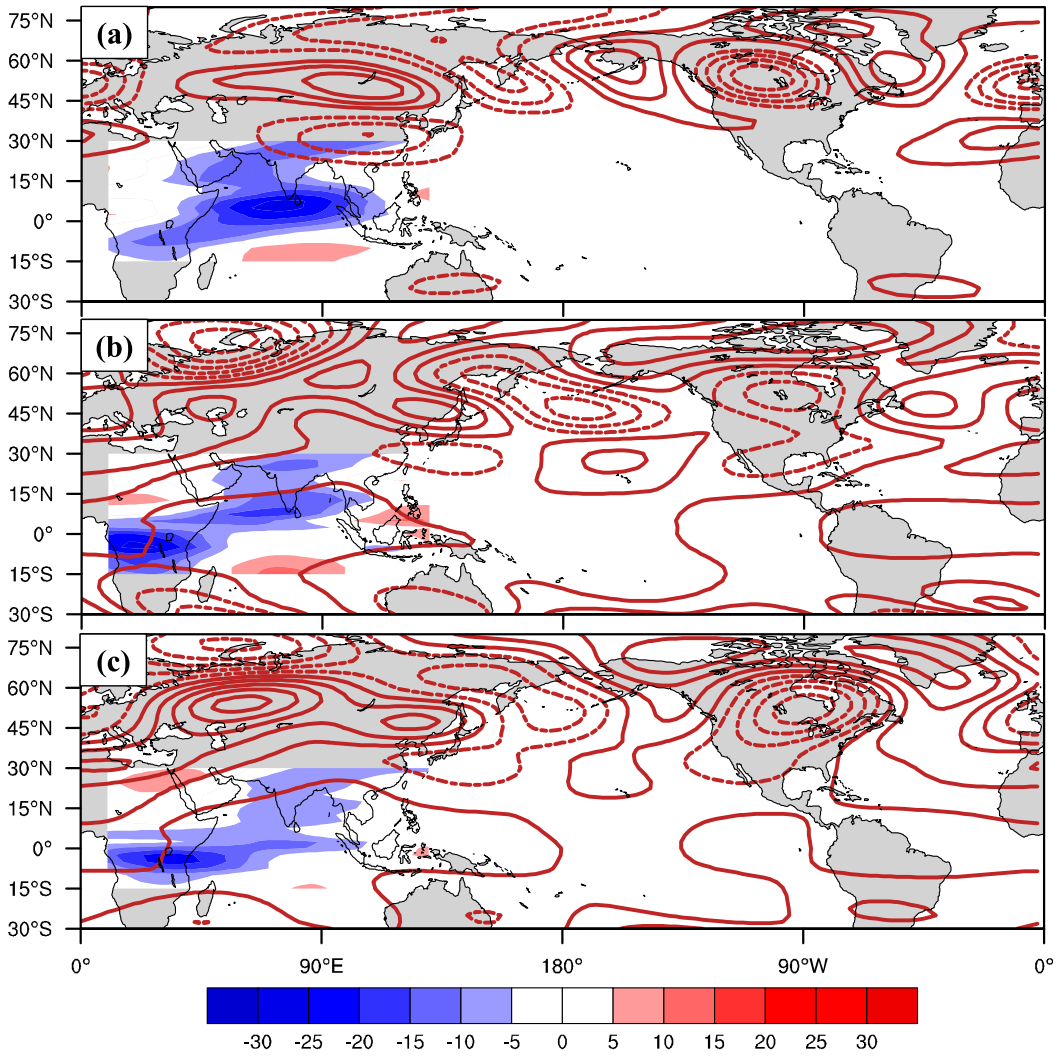

FIG. 11. Horizontal patterns of the MJO-related OLR (shading; W m^{-2}) in the tropical Indian Ocean and 200-hPa geopotential height (contours; gpm) on 29 Oct 2012, derived from (a) the observations, (b) prediction with initial condition on 23 Oct 2012, and (c) prediction with initial condition on 21 Oct 2012.

initial conditions. By comparing the model forecast fields with the observed counterparts, one can find that the difference between the two forecasts and the difference between the forecasts and the observations lie in proper representation of the northward propagation of the ISO signal from the tropical Atlantic and the remote teleconnection pattern forced by the tropical Indian Ocean. With the 23 October initial conditions, the model is capable of predicting the strength, location, and evolution characteristics of the ISO in the tropics and midlatitude regions.

The observational and modeling work above suggest that the extended-range forecast of TCs requires accurate predictions of atmospheric low-frequency motion such as the ISO. Thus it is crucial for operational models to improve MJO/ISO forecast skill. Most current state-of-the-art models, however, suffer large errors in MJO simulations (Jiang et al. 2015), possibly due to the model bias in capturing either MJO structure (Wang et al. 2017) or large-scale background state (Kim et al. 2011). Because the current study is just a case study, further studies with more cases and with a focus on specific processes through which the ISO influences TC genesis, intensity, and track are needed.

Recent studies (e.g., Hall and Sobel 2013; Lopeman et al. 2015; Lin et al. 2016) pointed out that Sandy was a very rare and extreme event with a return period of more than 100 years for flooding. The current study emphasizes that such an event requires the combination of the following factors: a TC with strong intensity and a northward track off the U.S. coast, a tropical Atlantic

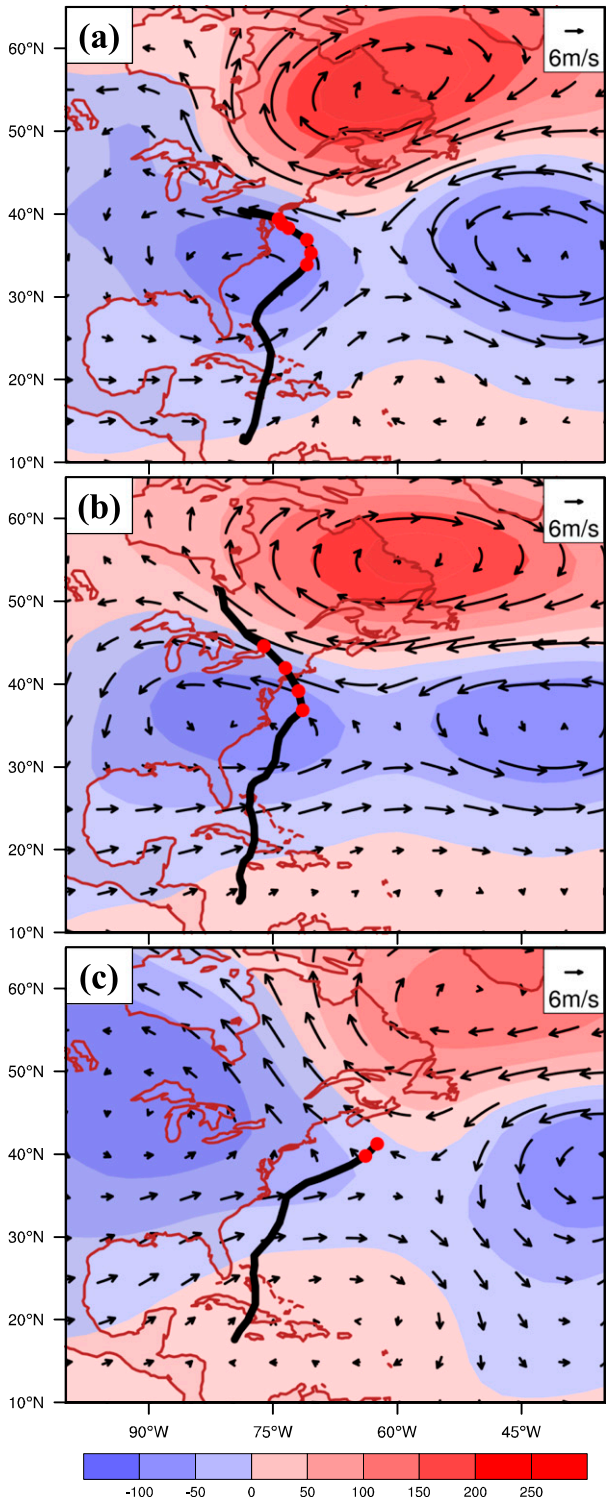

FIG. 12. Horizontal patterns of 850–200-hPa integrated low-frequency (10–90 day) steering-flow fields (vectors; m s^{-1}) and 500-hPa geopotential height (shading; gpm) on Oct 29 2012 derived from (a) the observations, (b) prediction with initial condition on 23 Oct 2012, and (c) prediction with initial condition on 21 Oct 2012. Black curves represent Sandy's tracks, and red dots denote Sandy's locations on 29 Oct 2012.

ISO that moves northward along with the TC, and a tropical Indian Ocean ISO that is strong enough to trigger a global Rossby wave train across Asia, the Pacific, and North America. It also partially explains why the prediction was very challenging for many operational centers around the world (e.g., NCEP).

TC movement in general is affected not only by the ISO but also by other low-frequency modes such as convectively coupled Kelvin and Rossby waves, the quasi-biweekly oscillation, and El Niño–Southern Oscillation. Thus a thorough analysis of various low-frequency modes on TC activity is needed. The effects of the different low-frequency modes on TC genesis, track, and intensity change need to be quantified.

Acknowledgments. This work was jointly supported by National Key R&D Program of China 2018YFC1505804 and 2015CB453200, NOAA NA18OAR4310298, National Science Foundation AGS-1643297, NSFC Grant 41875069, and Naval Research Laboratory Grant N00173-16-1-G906. This is SOEST contribution number 10764, IPRC contribution number 1397, and ESMC number 275.

REFERENCES

Barnes, E. A., L. M. Polvani, and A. H. Sobel, 2013: Model projections of atmospheric steering of Sandy-like superstorms. *Proc. Natl. Acad. Sci. USA*, **110**, 15 211–15 215, https://doi.org/10.1073/pnas.1308732110.

Barrett, B. S., and L. M. Leslie, 2009: Links between tropical cyclone activity and Madden–Julian oscillation phase in the North Atlantic and northeast Pacific basins. *Mon. Wea. Rev.*, **137**, 727–744, https://doi.org/10.1175/2008MWR2602.1.

Bi, M., T. Li, M. Peng, and X. Y. Shen, 2015: Interactions between Typhoon Megi (2010) and a low-frequency monsoon gyre. *J. Atmos. Sci.*, **72**, 2682–2702, https://doi.org/10.1175/JAS-D-14-0269.1.

Blake, E. S., T. B. Kimberlain, R. J. Berg, J. P. Cangialosi, and J. L. Beven II, 2013: Tropical cyclone report: Hurricane Sandy (AL182012) 22–29 October 2012. NOAA/National Hurricane Center Tech. Rep. AL182012, 157 pp., http://www.nhc.noaa.gov/data/tcr/AL182012_Sandy.pdf.

Cao, X., T. Li, M. Peng, W. Chen, and G. Chen, 2014: Effects of monsoon trough intraseasonal oscillation on tropical cyclogenesis over the western North Pacific. *J. Atmos. Sci.*, **71**, 4639–4660, https://doi.org/10.1175/JAS-D-13-0407.1.

Carr, L. E., III, and R. L. Elsberry, 1990: Observational evidence for predictions of tropical cyclone propagation relative to environmental steering. *J. Atmos. Sci.*, **47**, 542–546, https://doi.org/10.1175/1520-0469(1990)047<0542:OEFPOT>2.0.CO;2.

——, and ——, 1995: Monsoonal interactions leading to sudden tropical cyclone track changes. *Mon. Wea. Rev.*, **123**, 265–290, https://doi.org/10.1175/1520-0493(1995)123<0265:MILTST>2.0.CO;2.

Cassou, C., 2008: Intraseasonal interaction between the Madden–Julian oscillation and the North Atlantic Oscillation. *Nature*, **455**, 523, https://doi.org/10.1038/nature07286.

Chan, J. C. L., and W. M. Gray, 1982: Tropical cyclone movement and surrounding flow relationships. *Mon. Wea. Rev.*, **110**, 1354–1374, https://doi.org/10.1175/1520-0493(1982)110<1354:TCMASF>2.0.CO;2.

Chen, J.-H., and S.-J. Lin, 2013: Seasonal predictions of tropical cyclones using a 25-km resolution general circulation model. *J. Climate*, **26**, 380–398, https://doi.org/10.1175/JCLI-D-12-00061.1.

Chen, P., M. P. Hoerling, and R. M. Dole, 2001: The origin of the subtropical anticyclones. *J. Atmos. Sci.*, **58**, 1827–1835, https://doi.org/10.1175/1520-0469(2001)058<1827:TOOTSA>2.0.CO;2.

Ding, Q., and B. Wang, 2007: Intraseasonal teleconnection between the summer Eurasian wave train and the Indian monsoon. *J. Climate*, **20**, 3751–3767, https://doi.org/10.1175/JCLI4221.1.

Duchon, C. E., 1979: Lanczos filtering in one and two dimensions. *J. Appl. Meteor.*, **18**, 1016–1022, https://doi.org/10.1175/1520-0450(1979)018<1016:LFIOAT>2.0.CO;2.

Frank, W. M., and P. E. Roundy, 2006: The role of tropical waves in tropical cyclogenesis. *Mon. Wea. Rev.*, **134**, 2397–2417, https://doi.org/10.1175/MWR3204.1.

Fu, B., T. Li, M. Peng, and F. Weng, 2007: Analysis of tropical cyclogenesis in the western North Pacific for 2000 and 2001. *Wea. Forecasting*, **22**, 763–780, https://doi.org/10.1175/WAF1013.1.

Greene, C. H., J. A. Francis, and B. C. Monger, 2013: Superstorm Sandy: A series of unfortunate events? *Oceanography*, **26**, 8–9, https://doi.org/10.5670/oceanog.2013.11.

Hall, T. M., and A. H. Sobel, 2013: On the impact angle of Hurricane Sandy's New Jersey landfall. *Geophys. Res. Lett.*, **40**, 2312–2315, https://doi.org/10.1002/grl.50395.

Hartmann, D. L., and E. D. Maloney, 2001: The Madden–Julian oscillation, barotropic dynamics, and North Pacific tropical cyclone formation. Part II: Stochastic barotropic modeling. *J. Atmos. Sci.*, **58**, 2559–2570, https://doi.org/10.1175/1520-0469(2001)058<2559:TMJOBD>2.0.CO;2.

Held, I. M., and M. J. Suarez, 1994: A proposal for the intercomparison of the dynamical cores of atmospheric general circulation models. *Bull. Amer. Meteor. Soc.*, **75**, 1825–1830, https://doi.org/10.1175/1520-0477(1994)075<1825:APFTIO>2.0.CO;2.

Henderson, S. A., E. D. Maloney, and S. W. Son, 2017: Madden–Julian oscillation Pacific teleconnections: The impact of the basic state and MJO representation in general circulation models. *J. Climate*, **30**, 4567–4587, https://doi.org/10.1175/JCLI-D-16-0789.1.

Holland, G. J., 1983: Tropical cyclone motion: Environmental interaction plus a beta effect. *J. Atmos. Sci.*, **40**, 328–342, https://doi.org/10.1175/1520-0469(1983)040<0328:TCMEIP>2.0.CO;2.

Hoskins, B. J., and D. J. Karoly, 1981: The steady linear response of a spherical atmosphere to thermal and orographic forcing. *J. Atmos. Sci.*, **38**, 1179–1196, https://doi.org/10.1175/1520-0469(1981)038<1179:TSLROA>2.0.CO;2.

Hsu, P.-C., T. Li, and C.-H. Tsou, 2011: Interactions between boreal summer intraseasonal oscillations and synoptic-scale disturbances over the western North Pacific. Part I: Energetics diagnosis. *J. Climate*, **24**, 927–941, https://doi.org/10.1175/2010JCLI3833.1.

——, ——, L. You, J. Gao, and H. Ren, 2015: A spatial–temporal projection model for 10–30 day rainfall forecast in South China. *Climate Dyn.*, **44**, 1227–1244, https://doi.org/10.1007/s00382-014-2215-4.

Jarvinen, B. R., C. J. Neumann, and M. A. S. Davis, 1984: A tropical cyclone data tape for the North Atlantic Basin, 1886–1983: Contents, limitations and uses. NOAA Tech. Memo. NWS NHC 22, 21 pp., https://repository.library.noaa.gov/view/noaa/7069.

Jiang, X., and T. Li, 2005: Reinitiation of the boreal summer intraseasonal oscillation in the tropical Indian Ocean. *J. Climate*, **18**, 3777–3795, https://doi.org/10.1175/JCLI3516.1.

——, ——, and B. Wang, 2004: Structures and mechanisms of the northward propagating boreal summer intraseasonal oscillation. *J. Climate*, **17**, 1022–1039, https://doi.org/10.1175/1520-0442(2004)017<1022:SAMOTN>2.0.CO;2.

——, and Coauthors, 2015: Vertical structure and physical processes of the Madden–Julian oscillation: Exploring key model physics in climate simulations. *J. Geophys. Res. Atmos.*, **120**, 4718–4748, https://doi.org/10.1002/2014JD022375.

Kalnay, E., and Coauthors, 1996: The NCEP/NCAR 40-Year Reanalysis Project. *Bull. Amer. Meteor. Soc.*, **77**, 437–471, https://doi.org/10.1175/1520-0477(1996)077<0437:TNYRP>2.0.CO;2.

Kieper, M. E., C. W. Landsea, and J. L. Beven II, 2016: A reanalysis of Hurricane Camille. *Bull. Amer. Meteor. Soc.*, **97**, 367–384, https://doi.org/10.1175/BAMS-D-14-00137.1.

Kim, D., A. H. Sobel, E. D. Maloney, D. M. Frierson, and I. Kang, 2011: A systematic relationship between intraseasonal variability and mean state bias in AGCM simulations. *J. Climate*, **24**, 5506–5520, https://doi.org/10.1175/2011JCLI4177.1.

Klotzbach, P. J., 2010: On the Madden–Julian oscillation–Atlantic hurricane relationship. *J. Climate*, **23**, 282–293, https://doi.org/10.1175/2009JCLI2978.1.

Kossin, J. P., S. J. Camargo, and M. Sitkowski, 2010: Climate modulation of North Atlantic hurricane tracks. *J. Climate*, **23**, 3057–3076, https://doi.org/10.1175/2010JCLI3497.1.

Lackmann, G. M., 2015: Hurricane Sandy before 1900 and after 2100. *Bull. Amer. Meteor. Soc.*, **96**, 547–560, https://doi.org/10.1175/BAMS-D-14-00123.1.

Lau, K.-H., and N.-C. Lau, 1990: Observed structure and propagation characteristics of tropical summertime synoptic scale disturbances. *Mon. Wea. Rev.*, **118**, 1888–1913, https://doi.org/10.1175/1520-0493(1990)118<1888:OSAPCO>2.0.CO;2.

Lee, C. Y., S. J. Camargo, F. Vitart, A. H. Sobel, and M. K. Tippett, 2018: Subseasonal tropical cyclone genesis prediction and MJO in the S2S dataset. *Wea. Forecasting*, **33**, 967–988, https://doi.org/10.1175/WAF-D-17-0165.1.

Li, R. C. Y., and W. Zhou, 2013: Modulation of western North Pacific tropical cyclone activity by the ISO. Part I: Genesis and intensity. *J. Climate*, **26**, 2904–2918, https://doi.org/10.1175/JCLI-D-12-00210.1.

Li, T., 2006: Origin of the summertime synoptic-scale wave train in the western North Pacific. *J. Atmos. Sci.*, **63**, 1093–1102, https://doi.org/10.1175/JAS3676.1.

——, 2012: Synoptic and climatic aspects of tropical cyclogenesis in western North Pacific. *Cyclone: Formation, Triggers and Control*, K. Oouchi and H. Fudeyasu, Eds., Nova Science Publishers, 61–94.

——, 2014: Recent advance in understanding the dynamics of the Madden–Julian oscillation. *J. Meteor. Res.*, **28**, 1–33, https://doi.org/10.1007/S13351-014-3087-6.

——, and Y. Zhu, 1991: Analysis and modeling of tropical cyclone motion: I: Asymmetric structure and sudden change of tracks. *Sci. China*, **34**, 222–233.

——, and B. Fu, 2006: Tropical cyclogenesis associated with Rossby wave energy dispersion of a preexisting typhoon. Part I: Satellite data analyses. *J. Atmos. Sci.*, **63**, 1377–1389, https://doi.org/10.1175/JAS3692.1.

——, ——, X. Ge, B. Wang, M. Peng, 2003: Satellite data analysis and numerical simulation of tropical cyclone formation. *Geophys. Res. Lett.*, **30**, 2122, https://doi.org/10.1029/2003GL018556.

Liebmann, B., and C. A. Smith, 1996: Description of a complete (interpolated) outgoing longwave radiation dataset. *Bull. Amer. Meteor. Soc.*, **77**, 1275–1277.

Lin, H., G. Brunet, and J. Derome, 2009: An observed connection between the North Atlantic Oscillation and the Madden–Julian oscillation. *J. Climate*, **22**, 364–380, https://doi.org/10.1175/2008JCLI2515.1.

Lin, N., R. E. Kopp, B. P. Horton, and J. P. Donnelly, 2016: Hurricane Sandy's flood frequency increasing from year 1800 to 2100. *Proc. Natl. Acad. Sci. USA*, **113**, 12 071–12 075, https://doi.org/10.1073/pnas.1604386113.

Liu, Q., T. Li, and W.-C. Zhou, 2018: Impact of 10–60-day low-frequency steering flows on straight northward-moving typhoon tracks over the western North Pacific. *J. Meteor. Res.*, **32**, 394–409, https://doi.org/10.1007/s13351-018-7035-8.

Lopeman, M., G. Deodatis, and G. Franco, 2015: Extreme storm surge hazard estimation in lower Manhattan. *Nat. Hazards Rev.*, **78**, 355–391, https://doi.org/10.1007/s11069-015-1718-6.

Madden, R. A., and P. R. Julian, 1971: Detection of a 40–50 day oscillation in the zonal wind in the tropical Pacific. *J. Atmos. Sci.*, **28**, 702–708, https://doi.org/10.1175/1520-0469(1971)028<0702:DOADOI>2.0.CO;2.

——, and ——, 1972: Description of global-scale circulation cells in the tropics with a 40–50 day period. *J. Atmos. Sci.*, **29**, 1109–1123, https://doi.org/10.1175/1520-0469(1972)029<1109:DOGSCC>2.0.CO;2.

Maloney, E. D., 2000: Modulation of hurricane activity in the Gulf of Mexico by the Madden–Julian oscillation. *Science*, **287**, 2002–2004, https://doi.org/10.1126/science.287.5460.2002.

——, and D. L. Hartmann, 2000: Modulation of eastern North Pacific hurricanes by the Madden–Julian oscillation. *J. Climate*, **13**, 1451–1460, https://doi.org/10.1175/1520-0442(2000)013<1451:MOENPH>2.0.CO;2.

——, and M. J. Dickinson, 2003: The intraseasonal oscillation and the energetics of summertime tropical western North Pacific synoptic-scale disturbances. *J. Atmos. Sci.*, **60**, 2153–2168, https://doi.org/10.1175/1520-0469(2003)060<2153:TIOATE>2.0.CO;2.

Matthews, A. J., B. J. Hoskins, and M. Masutani, 2004: The global response to tropical heating in the Madden–Julian oscillation during the northern winter. *Quart. J. Roy. Meteor. Soc.*, **130**, 1991–2011, https://doi.org/10.1256/qj.02.123.

Mattingly, K. S., J. T. McLeod, J. A. Knox, J. M. Shepherd, and T. L. Mote, 2015: A climatological assessment of Greenland blocking conditions associated with the track of Hurricane Sandy and historical North Atlantic hurricanes. *Int. J. Climatol.*, **35**, 746–760, https://doi.org/10.1002/joc.4018.

Mo, K. C., 2000: The association between intraseasonal oscillations and tropical storms in the Atlantic basin. *Mon. Wea. Rev.*, **128**, 4097–4107, https://doi.org/10.1175/1520-0493(2000)129<4097:TABIOA>2.0.CO;2.

Pielke, R. A., J. Gratz, C. W. Landsea, D. Collins, M. A. Saunders, and R. Musulin, 2008: Normalized hurricane damage in the United States: 1900–2005. *Nat. Hazards Rev.*, **9**, 29–42, https://doi.org/10.1061/(ASCE)1527-6988(2008)9:1(29).

Qin, J., and W. A. Robinson, 1993: On the Rossby wave source and the steady linear response to tropical forcing. *J. Atmos. Sci.*, **50**, 1819–1823, https://doi.org/10.1175/1520-0469(1993)050<1819:OTRWSA>2.0.CO;2.

Rodrigues, R. R., and T. Woollings, 2017: Impact of atmospheric blocking on South America in austral summer. *J. Climate*, **30**, 1821–1837, https://doi.org/10.1175/JCLI-D-16-0493.1.

Sardeshmukh, P. D., and B. J. Hoskins, 1988: The generation of global rotational flow by steady idealized tropical divergence. *J. Atmos. Sci.*, **45**, 1228–1251, https://doi.org/10.1175/1520-0469(1988)045<1228:TGOGRF>2.0.CO;2.

Seo, K.-H., and S.-W. Son, 2012: The global atmospheric circulation response to tropical diabatic heating associated with the Madden–Julian oscillation during northern winter. *J. Atmos. Sci.*, **69**, 79–96, https://doi.org/10.1175/2011JAS3686.1.

Sobel, A. H., and E. D. Maloney, 2000: Effect of ENSO and the MJO on western North Pacific tropical cyclones. *Geophys. Res. Lett.*, **27**, 1739–1742, https://doi.org/10.1029/1999GL011043.

Sperber, K. R., J. M. Slingo, P. M. Inness, and W. K.-M. Lau, 1997: On the maintenance and initiation of the intraseasonal oscillation in the NCEP/NCAR reanalysis and in the GLA and UKMO AMIP simulations. *Climate Dyn.*, **13**, 769–795, https://doi.org/10.1007/S003820050197.

Takaya, K., and H. Nakamura, 2001: A formulation of a phase-independent wave-activity flux for stationary and migratory quasigeostrophic eddies on a zonally varying basic flow. *J. Atmos. Sci.*, **58**, 608–627, https://doi.org/10.1175/1520-0469(2001)058<0608:AFOAPI>2.0.CO;2.

Tam, C. Y., and T. Li, 2006: The origin and dispersion characteristics of the observed tropical summertime synoptic-scale waves over the western Pacific. *Mon. Wea. Rev.*, **134**, 1630–1646, https://doi.org/10.1175/MWR3147.1.

Vecchi, G. A., and Coauthors, 2014: On the seasonal forecasting of regional tropical cyclone activity. *J. Climate*, **27**, 7994–8016, https://doi.org/10.1175/JCLI-D-14-00158.1.

Wang, B., R. Wu, and T. Li, 2003: Atmosphere–warm ocean interaction and its impact on Asian–Australian monsoon variability. *J. Climate*, **16**, 1195–1211, https://doi.org/10.1175/1520-0442(2003)16<1195:AOIAII>2.0.CO;2.

Wang, L., T. Li, E. Maloney, and B. Wang, 2017: Fundamental causes of propagating and nonpropagating MJOs in MJOTF/GASS models. *J. Climate*, **30**, 3743–3769, https://doi.org/10.1175/JCLI-D-16-0765.1.

Wheeler, M. C., and G. N. Kiladis, 1999: Convectively coupled equatorial waves: Analysis of clouds and temperature in the wavenumber–frequency domain. *J. Atmos. Sci.*, **56**, 374–399, https://doi.org/10.1175/1520-0469(1999)056<0374:CCEWAO>2.0.CO;2.

——, and H. H. Hendon, 2004: An all-season real-time multivariate MJO index: Development of an index for monitoring and prediction. *Mon. Wea. Rev.*, **132**, 1917–1932, https://doi.org/10.1175/1520-0493(2004)132<1917:AARMMI>2.0.CO;2.

Xiang, B., and Coauthors, 2015a: Beyond weather time-scale prediction for Hurricane Sandy and Super Typhoon Haiyan in a global climate model. *Mon. Wea. Rev.*, **143**, 524–535, https://doi.org/10.1175/MWR-D-14-00227.1.

——, M. Zhao, X. Jiang, S.-J. Lin, T. Li, X. Fu, and G. Vecchi, 2015b: The 3–4-week MJO prediction skill in a GFDL coupled model. *J. Climate*, **28**, 5351–5364, https://doi.org/10.1175/JCLI-D-15-0102.1.

Zhao, C., and T. Li, 2019: Basin dependence of the MJO modulating tropical cyclone genesis. *Climate Dyn.*, **52**, 6081–6096, https://doi.org/10.1007/s00382-018-4502-y.

Zhao, M., and Coauthors, 2018: The GFDL Global Atmosphere and Land Model AM4.0/LM4.0: 1. Simulation characteristics with prescribed SSTs. *J. Adv. Model. Earth Syst.*, **10**, 691–734, https://doi.org/10.1002/2017MS001208.

Zhou, C., and T. Li, 2010: Upscale feedback of tropical synoptic variability to intraseasonal oscillations through the nonlinear rectification of the surface latent heat flux. *J. Climate*, **23**, 5738–5754, https://doi.org/10.1175/2010JCLI3468.1.

Zhu, Z., and T. Li, 2016: A new paradigm for continental U.S. summer rainfall variability: Asia–North America teleconnection. *J. Climate*, **29**, 7313–7327, https://doi.org/10.1175/JCLI-D-16-0137.1.